Epitaxial growth, structural and magnetic characterization of thulium thin films

Igor Lyalin [1], Katherine Robinson,[1] Alexander J. Bishop,[1] Gabriel Calderón Ortiz,[2]
Sadikul Alam,[2] Jinwoo Hwang,[2] and Roland K. Kawakami [1,*]

[1]*Department of Physics, The Ohio State University, Columbus, Ohio 43210, USA*
[2]*Department of Materials Science and Engineering, The Ohio State University, Columbus, Ohio 43210, USA*

Magnetic properties of bulk thulium crystals have been studied, with most works dating back to the 1960s, but to our knowledge, studies of thulium thin films are lacking. Here, we report the growth of Tm(0001) epitaxial films on SiC(0001) by means of molecular beam epitaxy. Clear Laue oscillations and narrow rocking curves in the x-ray diffraction scans indicate the high crystalline quality of the films. Magnetic circular dichroism and the anomalous Hall effect are utilized to probe magnetic properties. Periodic changes of remanent magnetization indicate a ferrimagnetic order with a period of seven monolayers along the c axis, in agreement with the ferrimagnetic properties of the bulk. The realization of Tm thin films opens the door to explore physics that could not be probed in the bulk.

I. INTRODUCTION

In recent years, studies of rare-earth (RE) elements (e.g., Eu, Gd, Tb, Er, Tm, etc.) as a part of more complex systems have attracted a lot of interest in spintronics research. Metallic ferrimagnetic alloys of RE elements with transition metals, such as GdFeCo, are of interest due to the demonstration of an ultrafast all-optical magnetization switching [1,2], observation of room-temperature skyrmions [3,4], and fast antiferromagneticlike magnetization dynamics near the angular momentum compensation temperature [5,6]. Another interesting class of materials based on RE is thin films of rare-earth iron garnets ($R_3Fe_5O_{12}$) which demonstrate efficient spin-orbit torque switching and fast domain wall motion when interfaced with a heavy metal [7–9]. They are attractive candidates for magnetic memory applications since their Gilbert damping constant is generally much lower than of metallic films which can enable low current density writing of magnetic bits.

One of the important characteristics of both materials discussed above is the ferrimagnetic (FiM) order, which is very appealing for spintronics as it combines some of the best properties of antiferromagnets (AFMs) and ferromagnets (FMs) [10]. As AFMs, their resonance frequencies are larger than FMs which enables, in principle, faster switching times for magnetic storage. At the same time, as FMs, they have nonzero magnetization which enables a more straightforward detection of the magnetic states compared to AFMs [11]. Thus, there is great interest in a fundamental understanding of FiMs and their magnetoelectronic properties.

Interestingly, elemental thulium is a RE metal that possesses FiM order on its own. It has a complex phase diagram that includes a FiM state with the magnetic moment modulated along the hexagonal c axis with a period of 7 monolayers

(ML) as shown in Fig. 1. Surprisingly, while properties of bulk thulium crystals have been studied, with most works dating back to the 1960s [12–16], to our knowledge, thin-film studies of this material are lacking.

In this paper, we develop the growth of Tm(0001) epitaxial films on SiC(0001) by means of molecular beam epitaxy (MBE) and report two interesting observations, namely, oscillations in remanent magnetization with a film thickness with a period of 7 ML and a giant-magnetoresistance (GMR)-like effect in magnetotransport. For the MBE growth, a combination of *in situ* reflection high-energy electron diffraction (RHEED) and x-ray diffraction (XRD) is used to identify the optimal growth temperature window. Clear Laue oscillations and narrow rocking curves in XRD scans indicate the high crystalline quality of the films. The magnetic properties of the grown films are investigated using magnetic circular dichroism (MCD), anomalous Hall effect (AHE), and magnetoresistance. The realization of Tm thin films opens the door to explore physics that could not be probed previously in the bulk and may lead to a better understanding of compound materials based on Tm.

II. GROWTH AND STRUCTURAL CHARACTERIZATION

Tm(0001) films were grown via MBE using a solid-source Tm effusion cell. 4H-SiC(0001) was chosen for the substrate due to a close lattice match between the two hexagonal crystal structures in the case of $30°$ in-plane rotation of the Tm lattice relative to SiC, $a_{Tm} = 3.534$ Å [17] and $a_{SiC} = 3.073$ Å [18]. In this case, the SiC lattice constant a_{SiC} would be approximately equal to $\sqrt{3}/2\,a_{Tm}$, yielding a $\sim 0.4\%$ tensile strain. Surprisingly, as discussed later, we observe that Tm(0001) grows with $0°$ in-plane rotation on SiC(0001). Thulium was grown at a variety of temperatures to investigate temperature dependence of crystal quality and determine the optimal growth. All samples, unless otherwise specified, were capped
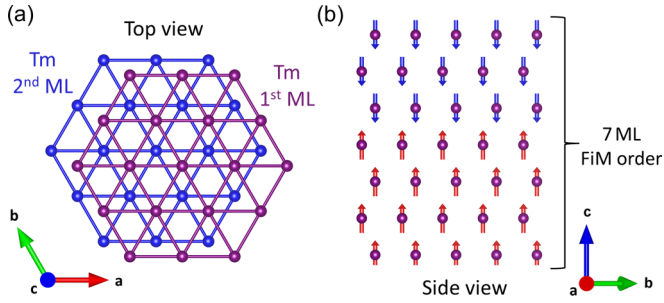
---
*kawakami.15@osu.edu

FIG. 1. (a) Schematics of the Tm hexagonal-closed-packed crystal structure. The first (purple) and second (blue) monolayers are shown. (b) 7-ML periodic ferrimagnetic order of Tm at low temperature: Magnetic moments are parallel to the c axis in four hexagonal layers followed by three layers with antiparallel moments (drawn using VESTA [20]).

with 5-nm CaF_2 (transparent insulator) to prevent oxidation of the films.

Figure 2(a) shows the *in situ* RHEED patterns of 17.5-nm-thick Tm(0001) films grown at different temperatures ranging from room temperature (RT) to 300 °C [see Supplemental Material (SM) Sec. S1 for more details [19]]. The RHEED pattern of the RT growth shows streaks but also rings, which are visible as increased intensity at the intersection with the streaks. These rings are indicative of polycrystalline domains. A higher temperature (100 °C) has a clear streaky RHEED pattern without rings, which indicates flat two-dimensional growth with finite terrace size. The 200 °C pattern is also streaky, but has faint spots along the streaks, suggesting a rougher surface with the formation of three-dimensional features. Growing at even higher temperatures (300 °C) further increases the three-dimensional (3D) features present, as evident by a spottier RHEED pattern. Therefore, based on RHEED alone, 100 °C seems to be the best growth temperature. The RHEED patterns shown in Fig. 2(a) are along the SiC[11$\bar{2}$0] direction. Based on the change by $\sim\sqrt{3}/2$ between the SiC RHEED spacing and Tm RHEED, we conclude that it is the [11$\bar{2}$0] direction for Tm as well. As mentioned above, this means that Tm grows without a 30° in-plane rotation on SiC.

The films grown at different temperatures were also studied by XRD using the Cu $K\alpha$ line (wavelength 1.5406 Å). 2θ-ω scans of nominal 17.5-nm film thickness are shown in Fig. 2(c). All scans have a Tm(0002) peak near $2\theta \approx 32°$ and a substrate peak SiC(0004) near $2\theta \approx 36°$. Both RT and 100 °C scans show multiple Laue oscillations, indicating that Tm films are smooth and highly ordered in the out-of-plane direction. The 200 °C scan shows weaker Laue oscillations, while for 300 °C growth Laue oscillations disappear, suggesting a degradation of the film quality. X-ray reflectivity (XRR) scans [Fig. 2(b)] confirm that the roughness of the films increases for higher growth temperatures. The fitting of XRR data yields a roughness of Tm top interface with a CaF_2 capping layer of 0.1, 0.1, 0.5, and 1.7 nm for growth temperatures of RT, 100 °C, 200 °C, and 300 °C, respectively. Based on the combination of the RHEED and XRD data we conclude that 100 °C is the optimal growth temperature. While the 2θ-ω scans carry information about the out-of-plane lattice
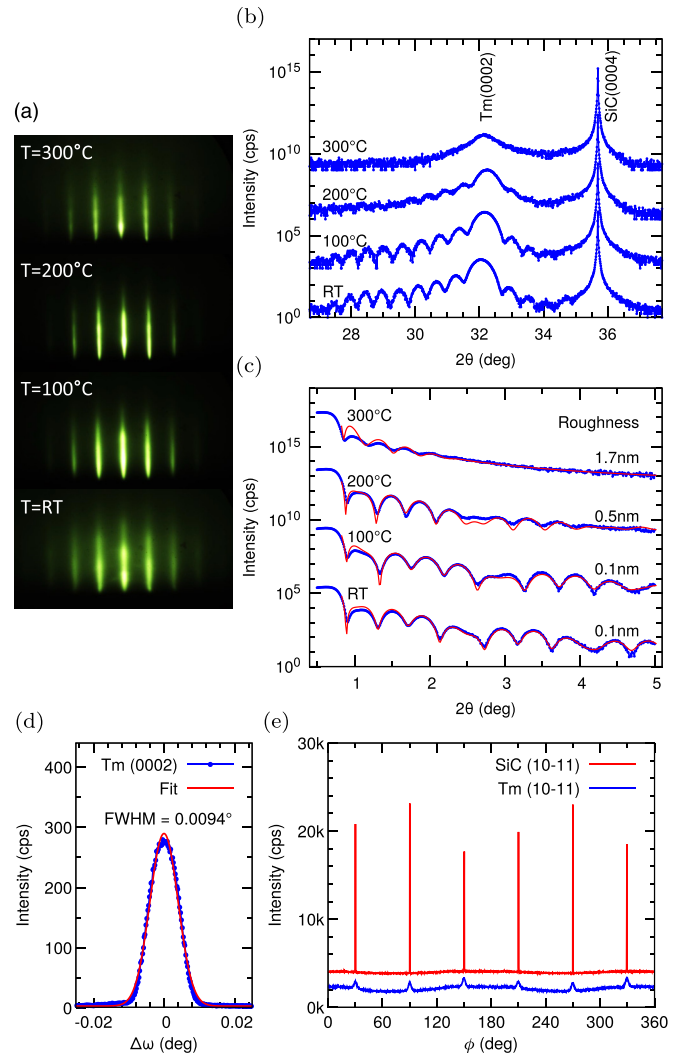

FIG. 2. Growth temperature dependence of Tm on 4H-SiC(0001): (a) RHEED patterns, (b) XRD 2θ-ω scans, and (c) XRR scans for 17.5-nm-thick Tm(0001) films. (d) XRD rocking curve of the Tm(0002) peak for the film grown at 100 °C. (e) XRD in-plane ϕ scan of SiC(10$\bar{1}$1) and Tm(10$\bar{1}$1) diffraction peaks showing sixfold in-plane symmetry and 0° relative rotation between SiC and Tm hexagonal lattices. The XRD and XRR data are offset along the vertical axes for clarity.

structure of Tm and suggest that RT and 100 °C growth are equally good, RHEED probes the in-plane lattice structure, indicating that films grown at 100 °C are more ordered.

To further probe the crystallinity of the Tm films, we performed XRD rocking curve scans on the Tm(0002) peak. For the 100 °C sample, shown in Fig. 2(d), a Gaussian fit yields the full width at half maximum (FWHM) of 0.0094°, which is very narrow for metallic epitaxial films, indicating a low spread of (0001) crystal planes relative to the sample normal (low mosaicity). The out-of-plane lattice constant extracted from the XRD analysis for the 100 °C growth temperature is $c = 5.56$ Å (1 ML = 2.78 Å), which agrees well with the reported bulk values of 5.573 Å [17] and 5.562 Å [21]. We also performed an in-plane XRD ϕ scan, shown in Fig. 2(e), and cross-sectional scanning transmission electron
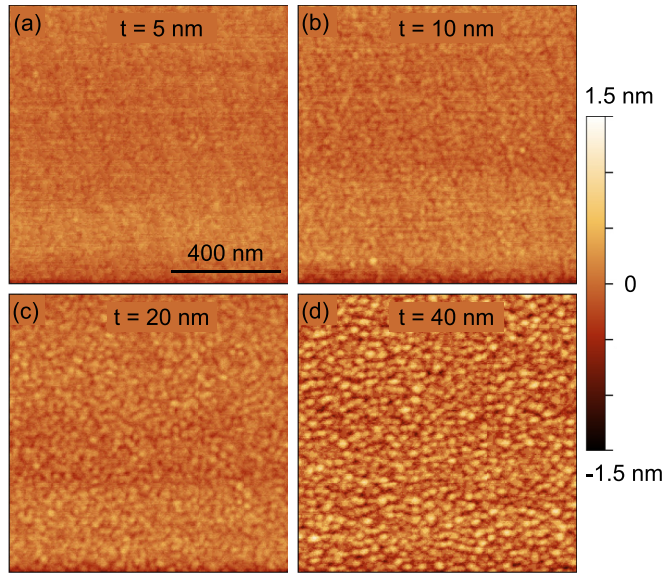
FIG. 3. AFM maps of Tm films for thicknesses: (a) $t = 5$ nm, the root-mean-square roughness $r_{rms} = 0.12$ nm, (b) $t = 10$ nm, $r_{rms} = 0.15$ nm, (c) $t = 20$ nm, $r_{rms} = 0.17$ nm, (d) $t = 40$ nm, $r_{rms} = 0.37$ nm.

microscopy (STEM), shown in SM Sec. S2 [19]. Both confirm the conclusion drawn from the RHEED analysis, namely, that the in-plane rotation angle between Tm and SiC unit cells is $0°$. Furthermore, STEM shows regions with different stacking sequences of the Tm planes. Both AB stacking expected for hexagonal-closed-packed (0001) planes and ABC stacking expected for face-centered-cubic (111) planes are observed. The $0°$ in-plane rotation, contradictory to the lattice match condition, calls for a detailed growth study of Tm thin films. We point out that other substrates can be suitable for the Tm(0001) growth, for instance, YSZ(111) with about 2% lattice mismatch.

To characterize the surface topography of the samples, in addition to XRR, we performed atomic force microscope (AFM) measurements on uncapped Tm films grown at $100\,°C$. The AFM data (Fig. 3) show that the samples have a flat surface, with a root-mean-square (rms) roughness of $r_{rms} = 0.17$ nm (approximately 2/3 ML) for a 20-nm-thick sample, which agrees with the roughness estimated from the XRR fitting. Performing AFM on films with different thickness, we observe that the surface roughness slightly increases for thicker films, from $r_{rms} = 0.12$ nm (for $t = 5$ nm) to $r_{rms} = 0.37$ nm (for $t = 40$ nm).

III. MAGNETIC AND MAGNETOTRANSPORT PROPERTIES

Although Tm has one of the lowest magnetic ordering temperatures among $4f$ rare-earth metals (56 K), it has an interesting, unusual, ferrimagnetic order. Below 32 K, the ferrimagnetic order is periodic, commensurable with the hexagonal crystal structure of thulium, magnetic moments are parallel to the c axis in four hexagonal layers followed by three layers with antiparallel moments [14] as shown in Fig. 1(b).
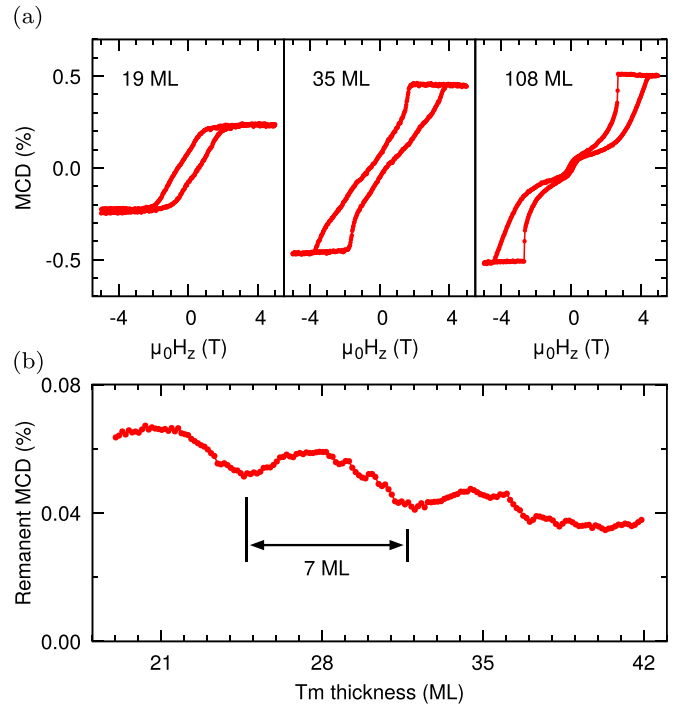

FIG. 4. Magnetic circular dichroism of Tm films at 2 K: (a) Out-of-plane hysteresis loops for 19-, 35-, and 108-ML-thick Tm films, and (b) remanent MCD ratio as a function of Tm thickness.

To investigate magnetic properties of the grown Tm films, we performed magnetic circular dichroism, anomalous Hall effect, and magnetoresistance measurements. To probe 7 ML periodicity of the ferrimagnetic order observed in the bulk, we grew several wedge samples and measured MCD as a function of the lateral position on a sample. This allowed us to study magnetic properties as a function of Tm thickness. For MCD measurements, we utilized a 800-nm laser light with an average power of 1 mW focused on a sample to a spot size of ∼70 µm. The helicity of the incident beam was modulated at 59 kHz by a photoelastic modulator and the MCD of the reflectivity was measured using an amplified Si photodiode and lock-in detection. Figure 4(a) shows three representative out-of-plane hysteresis loops for different Tm thicknesses (19, 35, and 108 ML) measured at 2 K. The hysteresis loop shape changes from a ferromagneticlike shape with the widest opening at zero field to a more antiferromagneticlike shape with a narrow middle part around 0 T and two symmetrical openings at large positive and negative fields, $\mu_0 H_z \approx 3$ T. This shape change is accompanied by the saturation field increase from about 2.0 to 4.2 T for thicknesses from $t = 5$ nm to $t = 30$ nm, while the remanent magnetization decreases from about 30% to 2%, suggesting a gradual transition from a more ferromagneticlike state to a more antiferromagneticlike state with increasing thickness. The saturation field of ∼4 T for the thick films agrees with the value for the bulk ∼3 T [22], but is somewhat larger. We estimate the penetration depth of the MCD measurement based on the variation of the MCD magnitude (at high field) as a function of film thickness, which plateaus above ∼10 nm [23].

Scanning a laser beam across a wedge allows us to measure the difference between MCD values after a positive (+5 T →
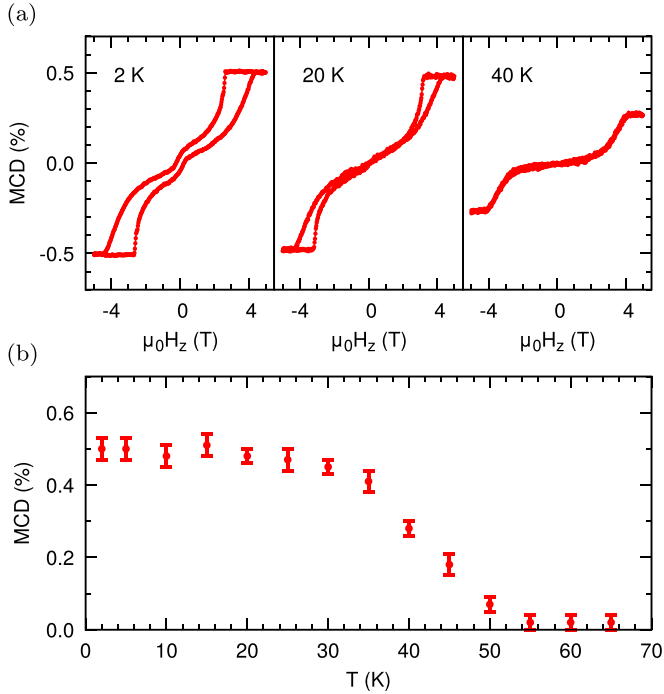
(a)

(b)

FIG. 5. Magnetic circular dichroism temperature dependence of a 20-nm-thick Tm film: (a) Out-of-plane hysteresis loops for 2, 20, and 40 K, and (b) MCD ratio as a function of temperature.

(a)   (b)

FIG. 6. Magnetotransport of a 20-nm-thick Tm film at 2 K: (a) Longitudinal resistivity ρ_{xx} and (b) transverse resistivity ρ_{xy} as a function of the out of the sample plane magnetic field.

One of the most interesting properties of Tm is magnetotransport. A detailed study of magnetoresistance in Tm bulk single crystals was conducted by Ellerby *et al.* [22]. Gigantic changes ($\sim$400%) of Tm resistance with current flow perpendicular to the hexagonal basal plane were observed. This large magnetoresistance ratio was explained by energy gaps opening in the band structure of Tm due to the periodic magnetic ordering, which leads to a reduction of the Fermi surface, and therefore to a higher electrical resistance state.

This model predicts that the in-plane resistivity, the case of Tm(0001) films, is affected only to the second order. The resistivity of a 20-nm Tm(0001) film grown in our work is 127 $\mu\Omega$ cm at room temperature and exhibits metallic behavior upon cooling down to 2 K. The residual resistivity ratio, defined as $\rho_{xx}(295 \text{ K})/\rho_{xx}(2 \text{ K})$, is 4.2, indicating a low defect density of the Tm films. Figure 6(a) shows a behavior of resistivity in magnetic field at $T = 2$ K. The resistivity at the high field, $\rho_{xx}(5 \text{ T}) \approx 29.3$ $\mu\Omega$ cm, is significantly lower than resistivity at the low field $\rho_{xx}(0 \text{ T}) \approx 32.7$ $\mu\Omega$ cm, which yields the magnetoresistance ratio of $\sim$10%. The magnitude of this value agrees with the energy gaps opening model given in Ref. [22]. We point out that, alternatively, by analogy with GMR in a $3d$ transition-metal multilayer [24–26], one could attribute this giant-magnetoresistance-like effect to spin-dependent scattering on antiferromagnetically coupled planes of Tm (current flow in the layer planes), since similar to $3d$ transition-metal multilayers, antiferromagnetic coupling in Tm and other heavy rare-earth metals is described by the Ruderman-Kittel-Kasuya-Yosida (RKKY) interaction [27]. We note that, to the best of our knowledge, GMR has not been observed to date in materials with solely $4f$ rare-earth metals [28].

In addition to the magnetoresistance, we measure the anomalous Hall effect in our Tm films. Figure 6(b) shows the Hall resistivity of a 20-nm film at $T = 2$ K. The AHE with the magnitude of anomalous Hall conductivity $\sigma_{xy} = \rho_{xy}/(\rho_{xx}^2) \approx 1.7 \times 10^4$ S/cm is observed. This value is 5–10 times smaller than AHE in Fe films of the same resistivity [29], or single-crystal Gd [30,31], but is comparable to the AHE in single-crystal Dy [32]. The sharp features in transverse resistivity ρ_{xy} at $\mu_0 H_z \approx \pm 2$ T can be attributed to the

0 T) and negative (-5 T $\rightarrow$ 0 T) magnetic field ramp, which is proportional to the remanent magnetization. The thickness step of the wedge in Fig. 4(b) is 1 ML with a lateral dimension of the step along the scanning direction of 158 μm, which is larger than the beam spot size. Periodic oscillations of remanent magnetization with a 7 ML period are observed in the range of 20–40 ML thickness [Fig. 4(b)]. The 7 ML periodicity of the remanent magnetization confirms the 7 ML FiM order in Tm, which was previously deduced from the neutron scattering experiments on the bulk [14]. The remanent MCD ratio decreases with the increased thickness and becomes virtually zero for films thicker than $\sim$80 ML. We also note that we observe an abrupt drop of the MCD magnitude for t thinner than 13 ML, with a hysteresis loop height being comparable to the noise level of the measurement for $t = 7$ ML. This suggests the existence of a few-ML-thick magnetically dead layer at the Tm/SiC interface. We speculate that the evolution of magnetic properties with thickness could be attributed to the interface with the SiC substrate. The interface can promote a ferromagnetic state in thin enough films (e.g., via epitaxial strain), while an increased roughness of the thicker films and stacking faults could average out the 7 ML ferrimagnetic periodicity, leading to an antiferromagneticlike state with zero net moment in zero field.

Figure 5 shows MCD temperature dependence of a 20-nm-thick Tm film. Representative out-of-plane MCD hysteresis loops for 2, 20, and 40 K are shown in Fig. 5(a). MCD saturation value as a function of temperature is plotted in Fig. 5(b). From this dependence we estimate a Néel temperature of about 55 K, consistent with the Néel temperature of the bulk [12–16].
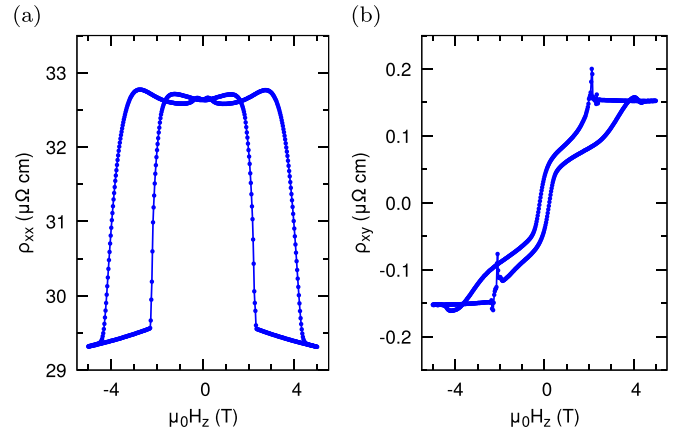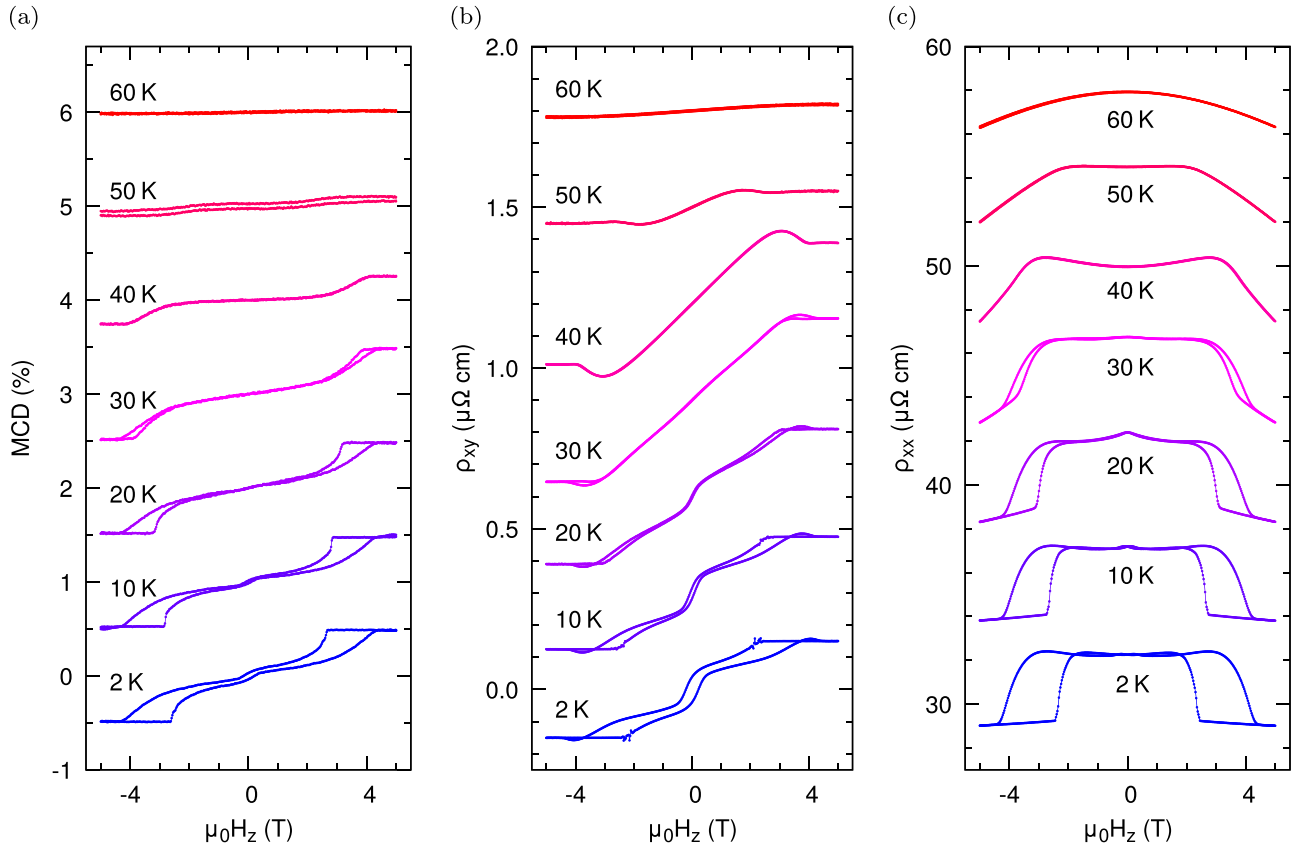
FIG. 7. Temperature-dependent MCD, transverse, and longitudinal resistivity of a 20-nm-thick Tm film: (a) MCD, (b) ρ_{xy}, (c) ρ_{xx}. The data are offset along the vertical direction for clarity of presentation. The MCD and ρ_{xy} data are antisymmetrized to exclude even in a magnetic field contribution from a slight sample motion in MCD measurements and from coupling to longitudinal resistivity in ρ_{xy} measurements.

planar Hall effect $\sim m_x m_y$, as these features have even symmetry with respect to the magnetic field. On the other hand, the gradual "overshooting" features with odd symmetry near $\mu_0 H_z \approx \pm 4$ T cannot be explained by the coupling between ρ_{xy} and ρ_{xx} due to the imperfect alignment of the Hall probes or the planar Hall effect. We note that these features become larger upon increasing T. The temperature dependence of transverse and longitudinal resistivity, as well as MCD, is shown in Fig. 7. These features and the difference between MCD and ρ_{xy} hysteresis loops shapes [Figs. 7(a) and 7(b)] can indicate the presence of a topological Hall effect in the Tm films due to topologically nontrivial magnetic textures (e.g., skyrmions), which would be an interesting study for future work. However, it is outside of the scope of the present study. See SM Sec. S3 for additional discussion [19].

IV. CONCLUSIONS

In conclusion, we have synthesized high-quality Tm(0001) thin films using molecular beam epitaxy. The structural properties of the films are characterized by a combination of RHEED, XRD, STEM, and AFM. Magnetic properties of the films are probed by MCD, AHE, and magnetoreistance measurements. The anomalous Hall conductivity of approximately 1.7×10^4 S/cm is measured and a 10% giant-magnetoresistance-like effect is observed in magnetotransport. Magnetic circular dichroism measurements reveal 7 ML periodicity of magnetic properties, observed previously only by neutron scattering experiments. The development of Tm films motivates more studies of this material and opens the door to the physics that could not be probed previously in the bulk.

[1] C. D. Stanciu, F. Hansteen, A. V. Kimel, A. Kirilyuk, A. Tsukamoto, A. Itoh, and T. Rasing, All-optical magnetic record-ing with circularly polarized light, Phys. Rev. Lett. **99**, 047601 (2007).

[2] K. Vahaplar, A. M. Kalashnikova, A. V. Kimel, D. Hinzke, U. Nowak, R. Chantrell, A. Tsukamoto, A. Itoh, A. Kirilyuk, and T. Rasing, Ultrafast path for optical magnetization reversal via a strongly nonequilibrium state, Phys. Rev. Lett. **103**, 117201 (2009).

[3] S. Woo, K. M. Song, X. Zhang, Y. Zhou, M. Ezawa, X. Liu, S. Finizio, J. Raabe, N. J. Lee, S.-I. Kim, S.-Y. Park, Y. Kim, J.-Y. Kim, D. Lee, O. Lee, J. W. Choi, B.-C. Min, H. C. Koo, and J. Chang, Current-driven dynamics and inhibition of the skyrmion Hall effect of ferrimagnetic skyrmions in GdFeCo films, Nat. Commun. **9**, 959 (2018).

[4] W. Legrand, D. Maccariello, F. Ajejas, S. Collin, A. Vecchiola, K. Bouzehouane, N. Reyren, V. Cros, and A. Fert, Room-temperature stabilization of antiferromagnetic skyrmions in synthetic antiferromagnets, Nat. Mater. **19**, 34 (2020).

[5] C. D. Stanciu, A. V. Kimel, F. Hansteen, A. Tsukamoto, A. Itoh, A. Kiriliyuk, and T. Rasing, Ultrafast spin dynamics across compensation points in ferrimagnetic GdFeCo: The role of angular momentum compensation, Phys. Rev. B **73**, 220402(R) (2006).

[6] K.-J. Kim, S. K. Kim, Y. Hirata, S.-H. Oh, T. Tono, D.-H. Kim, T. Okuno, W. S. Ham, S. Kim, G. Go, Y. Tserkovnyak, A. Tsukamoto, T. Moriyama, K.-J. Lee, and T. Ono, Fast domain wall motion in the vicinity of the angular momentum compensation temperature of ferrimagnets, Nat. Mater. **16**, 1187 (2017).

[7] C. O. Avci, E. Rosenberg, M. Baumgartner, L. Beran, A. Quindeau, P. Gambardella, C. A. Ross, and G. S. D. Beach, Fast switching and signature of efficient domain wall motion driven by spin-orbit torques in a perpendicular anisotropy magnetic insulator/Pt bilayer, Appl. Phys. Lett. **111**, 072406 (2017).

[8] S. Vélez, J. Schaab, M. S. Wörnle, M. Müller, E. Gradauskaite, P. Welter, C. Gutgsell, C. Nistor, C. L. Degen, M. Trassin, M. Fiebig, and P. Gambardella, High-speed domain wall racetracks in a magnetic insulator, Nat. Commun. **10**, 4750 (2019).

[9] L. Caretta, S.-H. Oh, T. Fakhrul, D.-K. Lee, B. H. Lee, S. K. Kim, C. A. Ross, K.-J. Lee, and G. S. D. Beach, Relativistic kinematics of a magnetic soliton, Science **370**, 1438 (2020).

[10] S. K. Kim, G. S. D. Beach, K.-J. Lee, T. Ono, T. Rasing, and H. Yang, Ferrimagnetic spintronics, Nat. Mater. **21**, 24 (2022).

[11] V. Baltz, A. Manchon, M. Tsoi, T. Moriyama, T. Ono, and Y. Tserkovnyak, Antiferromagnetic spintronics, Rev. Mod. Phys. **90**, 015005 (2018).

[12] B. L. Rhodes, S. Legvold, and F. H. Spedding, Magnetic properties of holmium and thulium metals, Phys. Rev. **109**, 1547 (1958).

[13] D. D. Davis and R. M. Bozorth, Magnetic properties of thulium metal, Phys. Rev. **118**, 1543 (1960).

[14] W. C. Koehler, J. W. Cable, E. O. Wollan, and M. K. Wilkinson, Magnetic structures of thulium, Phys. Rev. **126**, 1672 (1962).

[15] L. R. Edwards and S. Legvold, Transport properties of thulium single crystals, Phys. Rev. **176**, 753 (1968).

[16] T. O. Brun, S. K. Sinha, N. Wakabayashi, G. H. Lander, L. R. Edwards, and F. H. Spedding, Temperature dependence of the periodicity of the magnetic structure of thulium metal, Phys. Rev. B **1**, 1251 (1970).

[17] L.-G. Liu, W. A. Bassett, and M. S. Liu, High-pressure polymorph of thulium: An X-ray diffraction study, Science **180**, 298 (1973).

[18] Y. Goldberg, M. E. Levinshtein, and S. L. Rumyantsev, in *Properties of Advanced Semiconductor Materials: GaN, AIN, InN, BN, SiC, SiGe*, edited by M. E. Levinshtein, S. L. Rumyantsev, and M. S. Shur (Wiley, New York, 2001), pp. 93–148.

[19] See Supplemental Material at http://link.aps.org/supplemental/10.1103/PhysRevMaterials.8.054410 for details on the MBE growth, STEM data and analysis, and discussion of a possible topological Hall effect contribution, which includes Refs. [33,34].

[20] K. Momma and F. Izumi, VESTA 3 for three-dimensional visualization of crystal, volumetric and morphology data, J. Appl. Crystallogr. **44**, 1272 (2011).

[21] F. H. Spedding, J. J. Hanak, and A. H. Daane, High temperature allotropy and thermal expansion of the rare-earth metals, J. Less-Common Met. **3**, 110 (1961).

[22] M. Ellerby, K. A. McEwen, and J. Jensen, Magnetoresistance and magnetization study of thulium, Phys. Rev. B **57**, 8416 (1998).

[23] Z. Q. Qiu and S. D. Bader, Surface magneto-optic Kerr effect, Rev. Sci. Instrum. **71**, 1243 (2000).

[24] M. N. Baibich, J. M. Broto, A. Fert, F. Nguyen Van Dau, F. Petroff, P. Etienne, G. Creuzet, A. Friederich, and J. Chazelas, Giant magnetoresistance of (001)Fe/(001)Cr magnetic superlattices, Phys. Rev. Lett. **61**, 2472 (1988).

[25] G. Binasch, P. Grünberg, F. Saurenbach, and W. Zinn, Enhanced magnetoresistance in layered magnetic structures with antiferromagnetic interlayer exchange, Phys. Rev. B **39**, 4828(R) (1989).

[26] S. S. P. Parkin, Z. G. Li, and D. J. Smith, Giant magnetoresistance in antiferromagnetic Co/Cu multilayers, Appl. Phys. Lett. **58**, 2710 (1991).

[27] R. R. Gimaev, A. S. Komlev, A. S. Davydov, B. B. Kovalev, and V. I. Zverev, Magnetic and electronic properties of heavy lanthanides (Gd, Tb, Dy, Er, Ho, Tm), Crystals **11**, 82 (2021).

[28] F. E. Stanley, M. Perez, C. H. Marrows, S. Langridge, and B. J. Hickey, Inverse giant magnetoresistance in rare-earth/transition metal multilayers, Europhys. Lett. **49**, 528 (2000).

[29] S. Sangiao, L. Morellon, G. Simon, J. M. De Teresa, J. A. Pardo, J. Arbiol, and M. R. Ibarra, Anomalous Hall effect in Fe (001) epitaxial thin films over a wide range in conductivity, Phys. Rev. B **79**, 014431 (2009).

[30] R. S. Lee and S. Legvold, Hall effect of gadolinium, lutetium, and yttrium single crystals, Phys. Rev. **162**, 431 (1967).

[31] S. A. Baily and M. B. Salamon, Berry-phase contribution to the anomalous Hall effect in gadolinium, Phys. Rev. B **71**, 104407 (2005).

[32] J. J. Rhyne, Anomalous Hall effect in single-crystal dysprosium, Phys. Rev. **172**, 523 (1968).

[33] P. Bruno, V. K. Dugaev, and M. Taillefumier, Topological Hall effect and Berry phase in magnetic nanostructures, Phys. Rev. Lett. **93**, 096806 (2004).

[34] T. Liu, C. M. Selcu, B. Wang, N. Bagués, P.-K. Wu, T. Q. Hartnett, S. Cheng, D. Pelekhov, R. A. Bennett, J. P. Corbett, J. R. Repicky, B. McCullian, P. Chris Hammel, J. A. Gupta, M. Randeria, P. V. Balachandran, D. W. McComb, and R. K. Kawakami, An atomically tailored chiral magnet with small skyrmions at room temperature, Commun. Phys. **6**, 327 (2023).